CHEMBIOCHEM

DOI: 10.1002/cbic.200600075

# Myxovirescin A Biosynthesis is Directed by Hybrid Polyketide Synthases/Nonribosomal Peptide Synthetase, 3-Hydroxy-3-Methylglutaryl–CoA Synthases, and trans-Acting Acyltransferases

Vesna Simunovic, Josef Zapp, Shwan Rachid, Daniel Krug, Peter Meiser, and Rolf Müller*[a]

Myxococcus xanthus *DK1622 is shown to be a producer of myxovirescin (antibiotic TA) antibiotics. The myxovirescin biosynthetic gene cluster spans at least 21 open reading frames (ORFs) and covers a chromosomal region of approximately 83 kb. In silico analysis of myxovirescin ORFs in conjunction with genetic studies suggests the involvement of four type I polyketide synthases (PKSs; TaI, TaL, TaO, and TaP), one major hybrid PKS/NRPS (Ta-1), and a number of monofunctional enzymes similar to the ones involved in type II fatty-acid biosynthesis (FAB). Whereas deletion of either* taI *or* taL *causes a dramatic drop in myxovirescin production, deletion of both genes (Δ*taIL*) leads to the complete loss of myxovirescin production. These results suggest that both TaI and TaL PKSs might act in conjunction with a methyltransferase, reductases, and a monooxygenase to produce the 2-hydroxyvaleryl–S–ACP starter that is proposed to act as the biosynthetic primer in the initial condensation reaction with glycine. Polymerization of the remaining 11 acetates required for lactone formation is directed by 12 modules of Ta-1, TaO, and TaP megasynthetases. All modules, except for the first module of TaL, lack cognate acyltransferase (AT) domains. Furthermore, deletion of a discrete tandem AT—encoded by* taV*—blocks myxovirescin production; this suggests an "in trans" mode of action. To embellish the macrocycle with methyl and ethyl moieties, assembly of the myxovirescin scaffold is proposed to switch twice from PKS to 3-hydroxy-3-methylglutaryl–CoA (HMG–CoA)-like biochemistry during biosynthesis. Disruption of the S-adenosylmethionine (SAM)-dependent methyltransferase, TaQ, shifts production toward two novel myxovirescin analogues, designated myxovirescin $Q_a$ and myxovirescin $Q_c$. NMR analysis of purified myxovirescin $Q_a$ revealed the loss of the methoxy carbon atom. This novel analogue lacks bioactivity against* E. coli.

## Introduction

Type I polyketide synthases (PKS), nonribosomal peptide synthetases (NRPS), and their hybrids (PKS/NRPS) are multifunctional, multidomain enzymes responsible for the production of natural products by incorporation of small building blocks in assembly-line-like fashion that is analogous to animal fatty-acid biosynthesis (FAB).[1,2] In all three cases, the catalytic domains encoded within each module are responsible for the addition of one monomer unit to the growing chain, and its processing by various modification reactions. Typically, the fully extended product attached to the last module is dissociated from the megasynthetase to yield a free carboxylic acid or lactone structure, which undergoes further modifications by additional tailoring enzymes.

Whereas the unifying theme of PKS, NRPS, and FAB pathways is the catalytic flux of thioester-activated intermediates along the megasynthetase, differences in the choice of extender units and connecting bonds are reflected in the catalytic domains used to drive nonribosomal peptide (NRP), polyketide (PK), or fatty-acid (FA) chain elongation. For instance, formation of the peptide bond by NRPSs requires recognition and ATP-driven activation of two amino acids by their cognate adenylyation domains (A), coupling of the respective adenylated amino acids onto their downstream peptidyl-carrier proteins (PCP), and their final condensation by the condensation domain (C).[3] In PKS and FAB pathways, selection and loading of extender acyl units are executed by acyltransferases (AT). C–C bond formation between the two acyl groups attached to acyl carrier proteins (ACPs) is catalyzed by β-ketoacyl–ACP synthase (KS) by decarboxylative Claisen condensation. Unlike saturated FA biosynthesis, PKSs display greater variability in the

[a] *M.S. V. Simunovic, Dr. J. Zapp, Dr. S. Rachid, Dipl.-Chem. D. Krug, Apotheker P. Meiser, Prof. Dr. R. Müller*
*Saarland University, Pharmaceutical Biotechnology*
*Im Stadtwald, 66123 Saarbrücken (Germany)*
*Fax: (+49) 681-302-5473*
*E-mail: rom@mx.uni-saarland.de*

*Supporting information for this article is available on the WWW under http://www.chembiochem.org or from the author.*

level of β-ketothioester reduction, and can combine β-ketoacyl reductase (KR), β-hydroxyacyl dehydratase (DH), and enoyl reductase (ER). Additionally, PKSs might also perform methylations of carbon and oxygen[4] with *S*-adenosylmethionine (SAM)-dependent methyltransferases (MT). Carbon-specific methyltransferases couple the methyl group onto the activated α-carbon of the β-ketothioester intermediate, either during or postassembly of the natural product.

In contrast to the multifunctional type I PKSs and animal FAB megasynthases, FA biosynthesis in bacteria and higher plants is governed by monofunctional, iteratively-acting enzymes that are encoded as separate ORFs; these are designated type II FAB.[5] FAB in *E. coli* is initiated by KSIII (FabH), which performs the initial condensation of acetyl–CoA with malonyl–ACP to yield acetoacetyl–ACP. Two other β-ketoacyl–ACP synthases, KS I (FabF) and KAS II (FabB), carry out further elongation steps and show more specificity in their choice of substrates.[2,6–8]

A closer relationship between the type II FAB and PKS/NRPS-like natural product biosynthetic gene clusters came to light with the recent sequencing of pederin, mupirocin, and jamaicamide biosynthetic gene clusters.[9–12] In these systems type II FAB enzymes appear to act in concert with the type I PKS and NRP megasynthases to create potent natural products.

Myxovirescins (also known as antibiotic TA) are wide-spectrum antibiotics that are active against Gram-negative bacteria, and have to date been exclusively found in the genus *Myxococcus*.[13–16] In addition to their antimicrobial activity, myxovirescins are exceptionally adhesive to a variety of surfaces and dental tissues, which makes them good leads for the treatment of plaque and gingivitis in humans.[17–19] The sequencing of several ORFs that belong to the myxovirescin biosynthetic cluster in the red-pigmented *Myxococcus xanthus* strain ER-15, has been carried out. However, these studies have led to a great underestimation of the size of the biosynthetic gene cluster[20] and have failed to pinpoint the function of individual genes in myxovirescin biosynthesis, as polar effects of the described mutations could not be excluded.[20–24]

This is the first report on the identification, isolation, and structure elucidation of myxovirescin antibiotics from *M. xanthus* strain DK1622. Furthermore, based on the genome sequence of *M. xanthus* DK1622, we present the annotation of the complete myxovirescin biosynthetic gene cluster, propose its biosynthetic assembly, and by performing a series of in-frame gene deletions provide the first unambiguous genetic evidence for the involvement of certain genes in myxovirescin assembly. Finally, we demonstrate that *M. xanthus* DK1622 is a valuable genetic system for biosynthetic studies and genetic engineering of PKS/NRPS pathways, as disruption of the SAM-dependent methyltransferase, TaQ, leads to the production of two novel desmethyl analogues of myxovirescin.

## Results

### *M. xanthus* DK1622 produces myxovirescin antibiotics

The first hint that *M. xanthus* DK1622 could be a myxovirescin producer arose when we analyzed its genome for the presence of secondary-metabolite biosynthetic genes.[25] The genome was analyzed by performing a BLAST search with the previously reported PKS/NRPS fragment from *ta-1* from *M. xanthus* ER-15, which has been shown to be responsible for myxovirescin biosynthesis. The search revealed the presence of an almost identical gene in strain DK1622. Additionally, Ta-1 was identified by MALDI-TOF analysis in one of the fractions obtained in the membrane-separation experiments.[26] To find out whether *M. xanthus* DK1622 is indeed a myxovirescin producer, HPLC and MS analyses were carried out. These revealed two characteristic peaks with a UV maximum at 239 nm (Figure 1 A) and masses diagnostic of myxovirescin antibiotics.[27] Due to the fact that more than 30 myxovirescin analogues have been de-

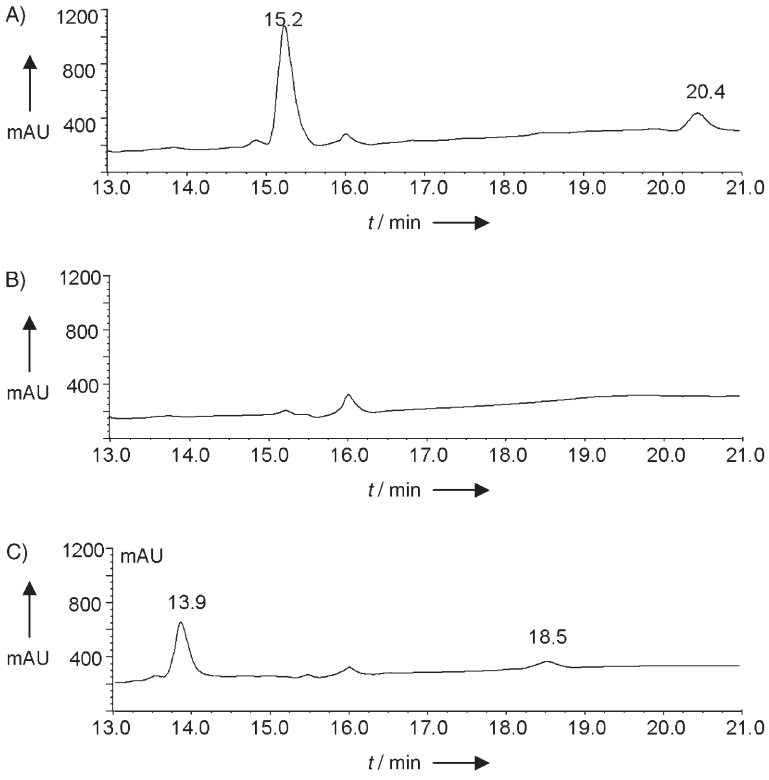


**Figure 1.** HPLC chromatogram traces of A) wild-type *M. xanthus* DK1622 strain, B) tandem acyltransferase mutant Δ*taV* (VS1017), and C) methyltransferase mutant *taQ* (VS1016) measured at 239 nm; **1** and **2** elute at 15.2 min and 20.4 min, respectively. *M. xanthus* VS1016 produced two novel metabolites with retention times of 13.9 and 18.5 min.

  

scribed from the related strain *M. virescens* Mx v48, we set out to perform a detailed chemical analysis of the two substances from strain DK1622.

### Structural analysis of myxovirescins produced by *M. xanthus* DK1622

According to high-resolution mass spectroscopy data and NMR analysis (Supporting Information), the two substances that showed retention times of 15.2 and 20.4 min (Figure 1 A) were identified as compounds **1** and **2** (Figure 2 A); NMR measurements were performed in $CD_3OD$.

### Analysis of the myxovirescin biosynthetic gene cluster

The myxovirescin biosynthetic gene cluster spans approximately 83 kb (Figure 2 B). It is dominated by four ORFs that encode type I PKSs (TaI, TaL, TaO, and TaP) and one major PKS/NRPS hybrid, Ta-1. Type I PKSs are flanked from both sides with various individual ORFs (*taA*–*taY* and *taQ*–*taS*), which show similarity to enzymes involved in type II FAS systems (*taV*, *taB-C*, *taE-F*, *taK*, *taX*, and *taY*). The closest homologues of myxovirescin ORFs were found in the biosynthetic gene clusters of pederin, mupirocin, and leinamycin (Table 1).[10,11,28]

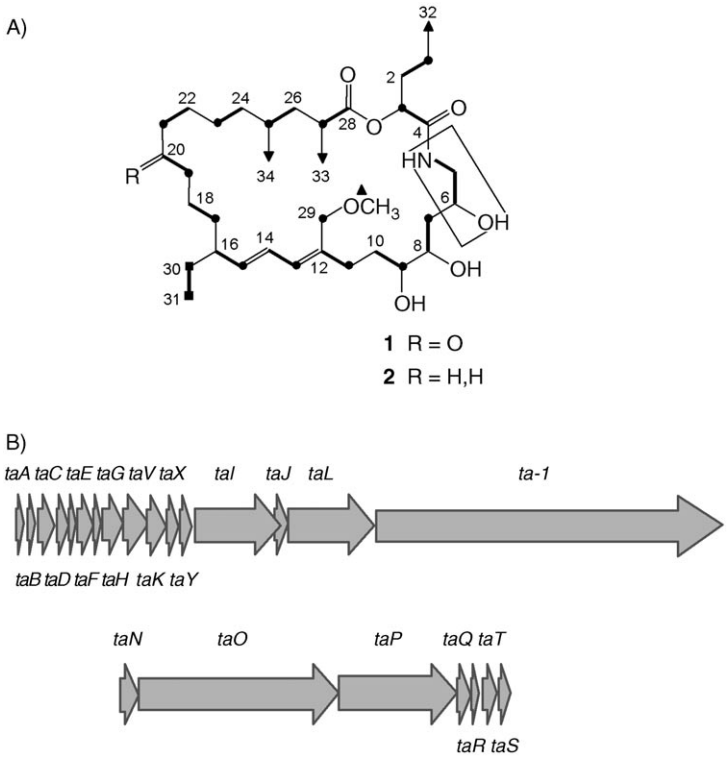


**Figure 2.** A) Stable isotope labeling of myxovirescin A (**1**), adopted from.[16] Myxovirescin C (**2**), the second major product, lacks the oxygen at C20. Boxed carbons originate from glycine, ● carbons indicate C2 of acetate, ▲ indicate methyl groups derived from methionine, and ■ show the ethyl groups that originates from succinate. B) Map of the 82.8 kb myxovirescin biosynthetic gene cluster.

### Analysis of domains that comprise the myxovirescin megasynthetase

β-*Ketoacyl synthases (KS)*: The myxovirescin biosynthetic gene cluster encodes 16 KS domains (Figure 3 A), 13 of which are conserved in the active-site Cys (box 1) and two His residues (boxes 2 and 3 in Figure 3 A).[29] Two KSs, TaL_KS1 (the first one found in TaL) and KS3, display a His to Gln substitution in the

**Table 1.** List of myxovirescin ORFs and their protein homologues.

| ORF | Protein/ gene | Size [Da/bp] | Putative function/homologue | Origin | Similarity/ identity [%] | Accession number of the protein homologue |
|---|---|---|---|---|---|---|
| 1 | TaA/*taA* | 18406/507 | transcription antiterminator | *Bacteriodes thetaiotaomicron* | 29/50 | AAO77992.1 |
| 2 | TaB/*taB* | 9270/252 | ACP | *Bacillus subtilis* subsp. *subtilis* strain 168 | 53/77 | NP_570904.1 |
| 3 | TaC/*taC* | 44851/1239 | HMG–CoA synthase PksG | *Bacillus subtilis* subsp. *subtilis* strain 168 | 66/80 | NP_389595.2 |
| 4 | TaD/*taD* | 34534/930 | unknown | | | |
| 5 | TaE/*taE* | 9170/252 | ACP | *Streptomyces atroolivaceus* | 41/67 | AAN85525.1 |
| 6 | TaF/*taF* | 46134/1263 | HMG–CoA synthase | *Streptomyces atroolivaceus* | 62/75 | AAN85526.1 |
| 7 | TaG/*taG* | 19599/516 | lipoprotein signal peptidase II | *Clostridium tetani* E88 | 35/57 | NP_782221.1 |
| 8 | TaH/*taH* | 53110/1428 | cytochrome P450-dependent enzyme | *Polyangium celullosum* | 38/56 | CAD43453.1 |
| 9 | TaV/*taV* | 71444/1974 | acyltransferase MmpIII | *Pseudomonas fluorescens* | 43/58 | AAM12912.1 |
| 10 | TaK | 43880/1254 | KS I/II PksF | *Bacillus subtilis* subsp. *subtilis* strain 168 | 54/72 | NP_389594.1 |
| 11 | TaX | 29229/789 | enoyl–CoA hydratase/isomerase | *Burkholderia mallei* ATTC 23344 | 56/71 | YP_105854.1 |
| 12 | TaY | 24880/666 | enoyl–CoA hydratase/isomerase PksI | *Bacillus subtilis* subsp. *subtilis* strain 168 | 65/79 | NP_389597.1 |
| 13 | TaI | 229067/6267 | Pks type I | symbiont bacterium of *Paederus fuscipes* | 37/51 | AAR19304.1 |
| 14 | TaJ | 43715/1179 | oxygenase OnnC | symbiont bacterium of *Theonella swinhoei* | 64/79 | AAV97871.1 |
| 15 | TaL | 235874/6549 | Pks type I | *Bacillus subtilis* subsp. *subtilis* strain 168 | 47/65 | NP_389602.2 |
| 16 | Ta-1/*ta-1* | 978123/27135 | OnnI PKS | symbiont bacterium of *Theonella swinhoei* | 44/60 | AAV97877.1 |
| 17 | TaN/*taN* | 53325/1458 | dioxygenase MmpIII | *Pseudomonas fluorescens* | 54/74 | AAM12912.1 |
| 18 | TaO/*taO* | 547875/15318 | Pks type I | *Bacillus subtilis* subsp. *subtilis* strain 168 | 47/65 | NP_389602.2 |
| 19 | TaP/*taP* | 330422/9114 | PksM polyketide synthase | *Bacillus subtilis* strain 168 | 35/53 | NP_389601.2 |
| 20 | TaQ/*taQ* | 35468/951 | SAM-dependent methyltransferase | *Mycobacterium tuberculosis* | 38/54 | NP_217468.1 |
| 21 | TaT/*taT* | 37567/1041 | unknown, containing DTW repeat domain | *Bdellovibrio Bacteriovorus HD 100* | 33/51 | CAE79280 |
| 22 | TaS/*taS* | 333/999 | radical SAM methyltransferase | *Clostridium beijerinckii* | 31/50 | AAS91673 |

  

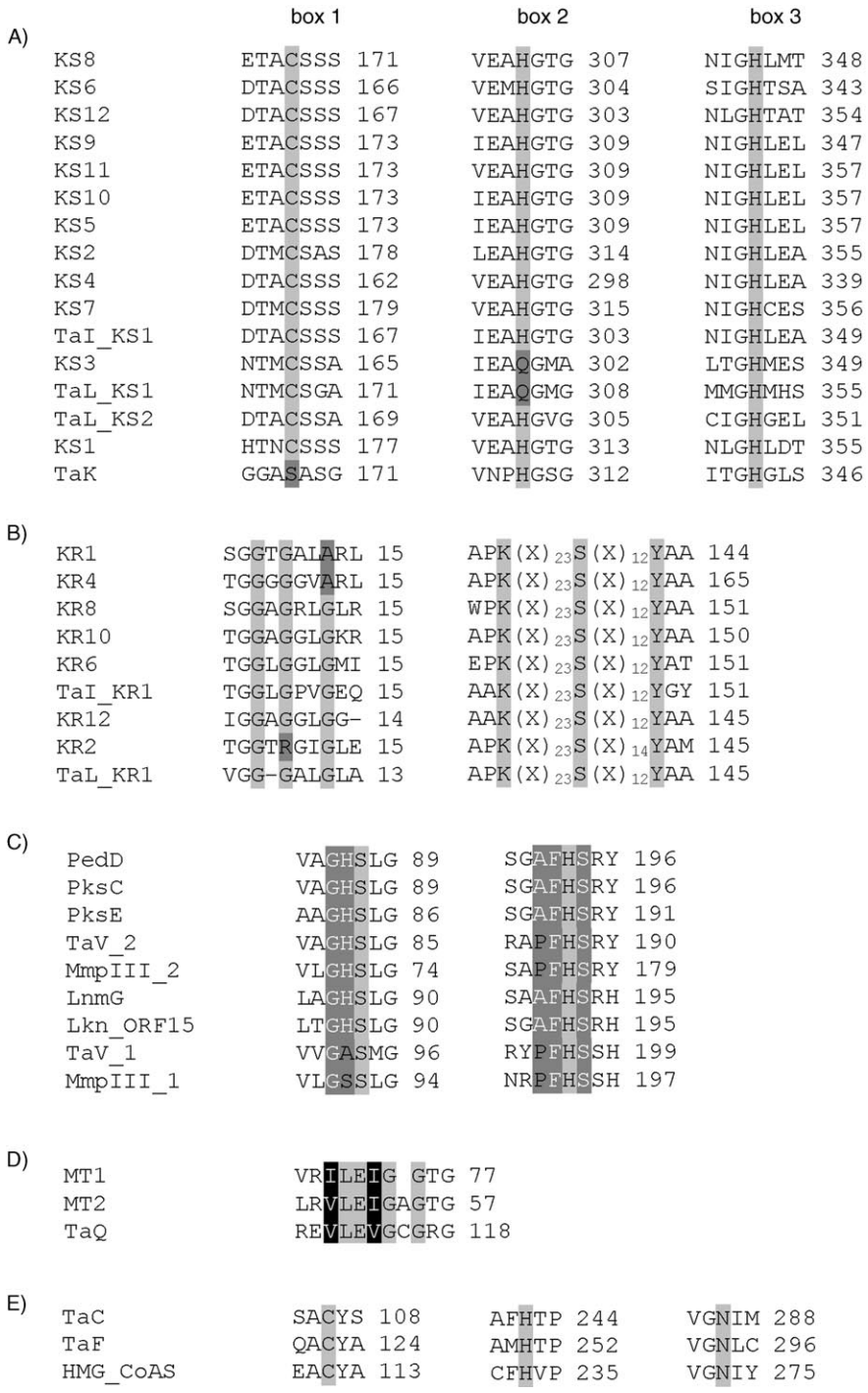


**Figure 3.** Clustal W alignments of the catalytic and conserved domains of: A) β-ketoacyl–ACP synthases (KS), B) β-ketoacyl–ACP reductases (KR), C) acyltransferases (AT), D) methyltransferase (MT), and E) 3-hydroxy-3-methylglutaryl–CoA (HMG–CoA) synthases. The active-site residues are shown in light gray, active-site substitutions are highlighted in dark gray, conserved residues are shown as white letters and are highlighted in dark gray, and similar amino acids are presented as white letters on a black background. The numbers indicate amino-acid positions within sequences and $(X)_n$ indicates the number of amino acids that separate the active-site residues. The accession numbers of acyltransferase homologues are given in parentheses: PedD from *Pederus beetles* (AAS47563), PksC and PksE from *B. subtilis* (NP_389591 and CAB13584), MmpIII from *Pseudomonas fluorescens* (AAM12912), LnmG from *Streptomyces atroolivaceus* (AAN85520), and ORF15 from *Streptomyces rochei* (NP_851437). The accession number of *Staphylococcus aureus* HMG–CoA synthase is AAG02422.

conserved box 2. However, TaK, the only discretely encoded β-ketoacyl–ACP synthase, carries a Cys to Ser substitution in the active site (Figure 3A).

*Ketoreductase (KR)*: Three ketoreductases, KR1, KR2, and KR4, display slight alterations in the Rosmann fold (GxGxxG), which is required for NADP(H) binding (Figure 3B). However, all nine KR domains contain the completely conserved Lys–Ser–Tyr catalytic triad that is necessary for ketoreduction.[30]

*Dehydratases (DH)*: All seven DH domains encoded in the cluster contain a conserved $His(X)_{13}Glu$ signature, in which His and Glu form a catalytic diad that is required for enzymatic activity.[29]

*Enoyl reductases (ER):* The myxovirescin cluster encodes two ER domains. Both of these show high identity with Zn-dependent alcohol dehydrogenases (Conserved domain search: COG1064), as well as with enoyl reductases from other systems. Whereas both ERs possess the conserved catalytic Tyr and Lys residues,[29] they occupy unusual positions within PKS modules (see below).

*Acyl-carrier proteins (ACP)*: All ACPs encoded in the cluster show the conserved catalytic Ser residue.

*Acyltransferases (AT)*: The myxovirescin cluster has only one atypical AT domain encoded within its functional modules (see below). Two more acyltransferases (AT1 and AT2; Table 2) are encoded discretely on the same open reading frame designated *taV*.

Both AT1 and AT2 contain a conserved active-site Ser, as well as a His residue that is specific for the binding of malonyl–CoA.[31] In a BLAST search, TaV showed the highest similarity to AT domains found in pederin, mupirocin, leinamycin, and lankacidin clusters (Figure 3C). All these biosynthetic gene clusters lack ATs as integral part of their modules and are referred to as "AT-less" or trans-AT type I PKSs;[32] instead, they contain separately encoded ATs that are thought to act iteratively. Recently, myxobacterial biosynthetic

  

**Table 2.** List of myxovirescin biosynthetic enzymes that contain PKS/NRPS domains.

| Protein | Size [Da] | | Encoded domains (coordinates in the protein sequence) |
|---|---|---|---|
| TaV | 71444 | | AT1 (1–330), AT2 (363–658) |
| TaK | 43880 | | $KS^S$ |
| TaI | 229067 | | GNAT (559–629), ACP (767–808) |
| | | | KS (839–1263), KR (1694–1875), |
| | | | ACP (2014–2079) |
| TaL | 235874 | | KS (32–460), KR (1091–1248), |
| | | | ACP (1344–1410) |
| | | | KS (1441–1867), ACP (2066–2132) |
| Ta-1 | 978123 | NRPS module | C (98–538), A (537–1041), |
| | | | PCP (1063–1125) |
| | | module 1 | KS1 (1154–1582), KR1 (1932–2109), |
| | | | ACP1 (2200–2257) |
| | | module 2 | KS2 (2300–2737), KR2 (3357–3543), |
| | | | ACP2 (3668–3724) |
| | | module 3 | KS3 (3759–4181), ACP3 (4391–4443) |
| | | module 4 | KS4 (4474–4893), KR4 (5547–5730), |
| | | | ACP4 (5823–5880) |
| | | module 5 | KS5 (5929–6365), ACP5 (6621–6680) |
| | | module 6 | KS6 (6736–7155), DH6 (7360–7511), |
| | | | KR6 (7819–8002), ACP6 (8097–8152) |
| | | module 7 | KS7 (8198–8634), ACP7 (8938–8997) |
| TaO | 547875 | module 8 | ER8 (58–356), KS8 (409–831), |
| | | | DH8 (1041–1179), KR8 (1474–1662), |
| | | | ACP8 (1759–1812) |
| | | module 9 | KS9 (1873–2309), DH9 (2500–2666), |
| | | | ACP9 (2830–2886) |
| | | module 10 | KS10 (2945–3381), DH10 (3564–3736), |
| | | | KR10 (4027–4226), ACP10 (4327–4384), |
| | | | KS10 (4458–4893) |
| TaP | 330422 | module 11 | MT11 (101–382), ACP11 (399–446) |
| | | module 12 | KS12 (502–922), KR12 (1615–1799), |
| | | | MT12 (2008–2280), ACP12 (2294–2345), |
| | | | ER12 (2294–2345), TE12 (2756–2919) |

gene clusters responsible for the production of disorazol and chivosazol have also been reported to have such gene organization.[33,34] Nevertheless, only mupirocin and myxovirescin biosynthetic gene clusters contain two AT domains that are encoded as one ORF.

*Methyltransferases (MT)*: Even though feeding studies with $^{13}C$-labeled precursors indicate the incorporation of four methyl groups (derived from methionine) into myxovirescin[16] (Figure 2A), only three putative SAM-dependent MT domains are found to be encoded in the cluster. Two of these MT domains, MT11 and MT12, are located within modules 11 and 12 of TaP (Table 2). The third putative SAM-dependent MT is encoded by *taQ*, which is immediately downstream of *taP*. All three MTs contain the conserved SAM-binding motif, V(I)LEV-(I)GXG[35] (Figure 3D). The only candidate that can carry out the fourth methylation is TaS, and the corresponding gene is located at the 3′ end of the cluster, about 2.7 kb downstream of *taQ* (Figure 2A).

*HMG–CoA synthases/β-ketoacyl–ACP synthase III (FabH)*: The *taC* and *taF* gene products show similarity to HMG–CoA synthases and β-ketoacyl–ACP synthases III (FabH). The closest homologues of TaC are putative HMG–CoA synthases (PksG) from *Bacillus subtilis* subsp. *subtilis* strain 168 (66% identity, 80% similarity) and JamH from *Lyngbya majuscula* (64% identity, 77% similarity). TaF shares the highest similarity with the putative HMG–CoA synthases LnmM, from *Streptomyces atroolivaceus* (62% identity, 75% similarity), and CurD from *L. majuscule* (47% identity, 65% similarity). Furthermore, both TaC and TaF share the conserved Cys–His–Asp catalytic triad with numerous HMG–CoA synthases that are involved in the mevalonate pathway, including that from *Streptococcus aureus* (Figure 3E).[36]

## Genetic analysis of the myxovirescin biosynthetic gene cluster

To elucidate the function of individual genes in myxovirescin biosynthesis, large regions of *taV* that encode the AT1 and AT2 domains, as well as large regions of *taI* and *taL* PKSs, were deleted in-frame in order to ensure the absence of polar effects on downstream ORFs (Tables 2 and 3). In addition, the putative methyltransferase, *taQ*, which is located at the very end of the gene cluster (Figure 2B), was disrupted by plasmid insertion. Wild-type DK1622 and mutant cells that were fermented with XAD adsorbent resin were extracted with methanol (see Experimental Section) and analyzed by HPLC. Unlike wild-type *M. xanthus* DK1622, which produces myxovirescins A and C (Figure 1A), both Δ*taV* (VS1017) and *taQ* (VS1016) mutant extracts showed loss of myxovirescin production (Figure 1B and C). In addition, the *taQ* knockout produced two novel metabolites with retention times of 13.9 and 18.5 min (Figure 1C); these were found to be in the same 5:1 ratio as **1** and **2** in the wild-type cells.

Investigation of Δ*taI* and Δ*taL* mutant extracts by LC-MS revealed that both *M. xanthus* strains VS1024 and VS1025 display a dramatic drop in antibiotic production compared to the wild-type cells (Figure 4A–C). In order to determine their exact concentrations, we developed a quantitative LC-MS method that can quantify **1** down to 1 ng mL$^{-1}$ (Experimental Section). Using this method, we measured an approximately 100000-fold drop in myxovirescin production in both Δ*taI* and Δ*taL* mutants, in comparison to wild-type production levels (data not shown). To test whether myxovirescin production persists in the absence of both TaI and TaL PKSs, a double Δ*talL* mutant was created (VS1029) and analyzed in the same fashion. Deletion of large regions of both genes in strain VS1029 clearly led to complete abolishment of myxovirescin production (Figure 4D).

## TaQ is an *O*-methyltransferase specific for the C29 oxygen

In order to elucidate the role of *taQ* methyltransferase, the novel product with the 13.9 min retention time (Figure 1C; exact mass of 610.43248 $[M+H]^+$ and molecular formula $C_{34}H_{60}NO_8$) was purified from XAD-adsorbent beads that were cofermented with *M. xanthus* VS1016 culture (8 L), and used for detailed NMR analysis (Table 4).

MS analysis confirmed the postulated loss of *m/z* 14 expected for the loss of one methyl group. In addition, $^1H$ and $^{13}C$ NMR spectroscopy data of **3** (Scheme 1A and Table 4) were

  

**Table 3.** List of plasmids and strains used in the study.

| Plasmid | Description of construction |
|---|---|
| pVS23 | 639 bp PCR product amplified by using primer pair taV1 and taV2, which contained *Not*I and *Spe*I restriction sites, respectively, and cloned into pCR2.1-TOPO |
| pVS26 | 662 bp PCR product amplified by using primer pair taV3 and taV4, which contained *Spe*I and *Sac*I sites, respectively, and cloned into pCR2.1-TOPO |
| pVS27 | 1295 bp fragment derived by ligating the 639 bp insert from pVS23 (digested with *Not*I and *Spe*I) with the 662 bp insert from pVS26 (digested with *Spe*I and *Sac*I); product was cloned into the *Not*I and *Spe*I sites of pSWU41 |
| pVS50 | 580 bp PCR product generated by using primer pair taI1 and taI2, which contained *Xba*I and *Bam*HI sites, respectively, and cloned into pCR2.1-TOPO |
| pVS51 | 578 bp PCR product generated by using primer pair taI3 and taI4, which contained *Bam*HI and *Spe*I sites, respectively, and cloned into pCR2.1-TOPO |
| pVS52 | 1152 bp fragment derived by ligating the 580 bp insert from pVS50 (digested with *Xba*I and *Bam*HI) and the 578 bp insert from pVS51 (digested with *Bam*HI and *Spe*I); product was cloned into the *Xba*I and *Spe*I sites of pSWU41 |
| pVS48 | 564 bp PCR product generated by using primer pair taL1 and taL2, which contained *Xba*I and *Bam*HI sites, respectively, and cloned into pCR2.1-TOPO |
| pVS49 | 563 bp PCR product generated by using primer pair taL3 and taL4, which contained *Bam*HI and *Spe*I sites, respectively, and cloned into pCR2.1-TOPO |
| pVS61 | 1121 bp fragment derived by ligating the 564 bp insert from pVS48 (digested with *Xba*I and *Bam*HI) and the 563 bp insert from pVS49 (digested with *Bam*HI and *Spe*I); product was cloned into the *Xba*I and *Spe*I sites of pSWU41 |
| pVS16 | 450 bp PCR product amplified by using the taQ_knock_frw and taQ_knock_rev primer pair, and cloned in pCR2.1-TOPO |
| pVS75 | 824 bp PCR product amplified by using taOseq_up and taOseq_down primer pair, and cloned into pCR2.1-TOPO |
| *M. xanthus* strains | genotype description |
| DK1622 | – |
| VS1017 (Δ*taV*) | Δ1455 bp encoding for AT1 and AT2 |
| VS1024 (Δ*taI*) | Δ4044 bp encoding for ACP–KS–KR–ACP domains |
| VS1025 (Δ*taL*) | Δ2382 bp encoding for ACP–KS–ACP domains |
| VS1029 (Δ*talL*) | Δ4044 bp encoding for ACP–KS–KR–ACP of *taI* and Δ2382 bp encoding for ACP–KS–ACP of *taL* |
| VS1016 (*taQ*) | merodiploid mutant created by homologous recombination of pVS16 into the genome of *M. xanthus* DK1622 |

similar to those observed for myxovirescin A,[37] and revealed C20 and C4 ketones ($\delta_C = 212.5$ and $\delta_C = 171.6$, respectively), a C28 ester ($\delta_C = 175.8$), and a secondary amide ($\delta_H = 6.78$), together with four secondary alcohols specific to carbons C3, C6, C8, and C9. Overall, the upper part of **3** was found to be in good agreement with that of **1**, whereas the lower part of the molecule (C5–C15, including C29) indicated structural changes. In addition, the spectra of **3** lacked signals for a methoxy group. Moreover, an additional resonance specific for a secondary alcohol connected to C13 appeared at $\delta_C = 80.6$ and $\delta_H = 4.21$. Another deviation between the two compounds was specific to the positions of two double bonds. Whereas **1** displays a conjugated, disubstituted system specific to C12 and C14 in the macrocycle, careful analysis of the chemical shifts of **3** revealed two isolated double bonds; one of them comprised an *exo*-methylene group made of a quaternary carbon C12 ($\delta_C = 146.4$,) and C29 (t, $\delta_C = 108.3$; $\delta_H = 4.79$ and 4.77, both br s).

The structure of the C5–C15 fragment, which includes C29, was deduced from $^1$H,$^1$H COSY and HSQC spectra. This allowed the construction of the two fragments shown in bold in Scheme 1 A. The first fragment (C12–C16) contains two double bonds separated by a secondary-alcohol function at C13. In the $^1$H,$^1$H COSY, two *exo*-methylene protons of C29 showed long-range couplings to the broad doublet of the methine proton of C13, which displayed further vicinal correlation to the olefinic proton of C14 at $\delta_H = 5.50$. The other olefinic proton ($\delta_H = 5.30$) showed the same neighborhood as in **1** and was therefore assigned to C15. The $^1$H,$^1$H COSY of the second fragment (C5–C11) indicated a complete conservation of the connectivity in this part of the molecule.

The confirmation of the structure for **3** was performed by using NMR prediction tools, which calculated similar resonance values for the respective carbon and hydrogen atoms. To our surprise, the *O*-desmethyl analogue of **1** failed to inhibit *E. coli* growth in the standard antibiotic assay (Figure 5).

## Discussion

### Proposed biosynthesis of myxovirescin A

### The myxovirescin gene cluster belongs to the trans-AT type of natural product biosynthetic gene clusters

All modules of the myxovirescin biosynthetic gene cluster—with the exception of the first module of TaI—lack AT domains. Instead, two acyltransferase domains are encoded by *taV* (Table 2). Based on the biochemical evidence that indicates the "trans" activity of acyltransferase LnmG of the leinamycin system, which is shown to load malonyl–CoA on every ACP of leinamycin megasynthetase,[38] we assumed a similar function for TaV. This hypothesis was confirmed by an in-frame deletion of *taV*, which led to a myxovirescin-negative phenotype (Figure 1 B).

### Starter biosynthesis

Feeding studies and the overall organization of the myxovirescin gene cluster suggest that biosynthesis of the myxovirescin starter unit takes place by fusion of an acetyl–S–ACP with malonyl–S–ACP. This is followed by subsequent methylation of the C1 carbon, reductions of C2, and hydroxylation of C3 (Scheme 2). The likely candidates for the first biosynthetic step are one or both of the first two modular PKSs, TaI and TaL.

TaI contains a peculiar GNAT domain (see below), followed by ACP–KS–KR–ACP domains. The GNAT superfamily of acetyltransferases perform nitrogen-specific acetylation reactions on a wide range of substrates, including glycosides, either to

  

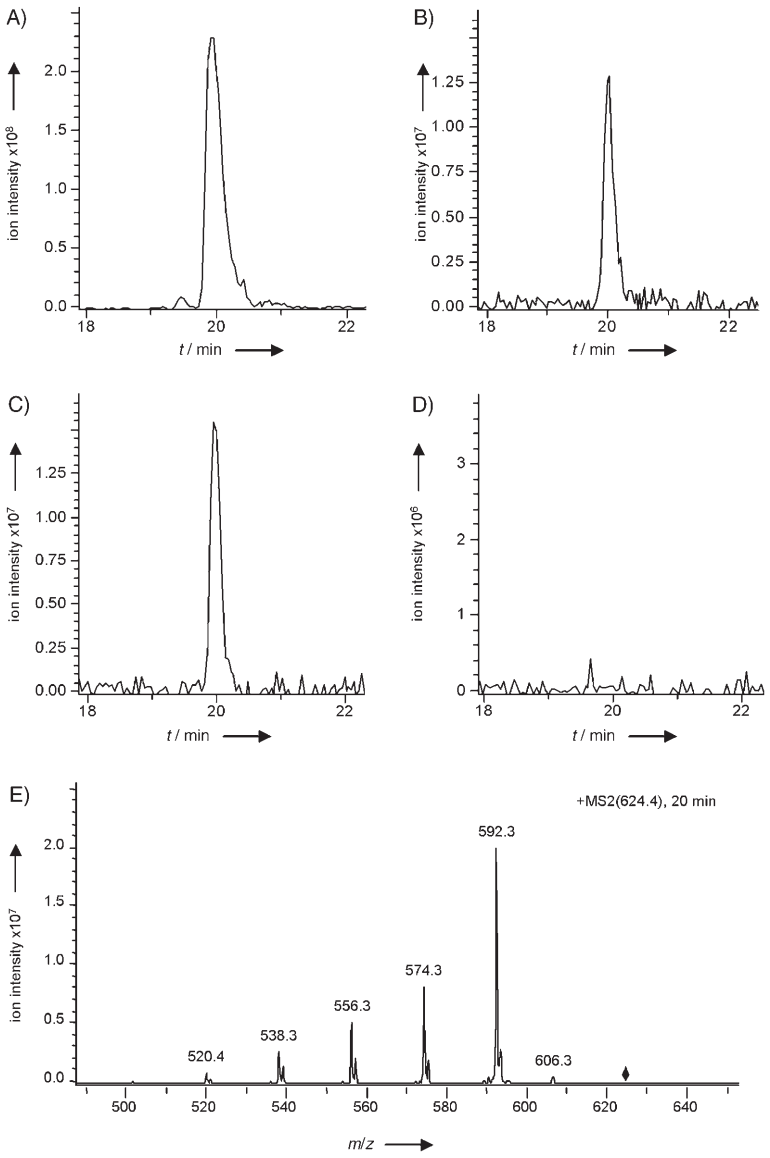


**Figure 4.** Extracted ion-mass chromatograms (EIC) of myxovirescin A from A) wild-type DK1622, B) Δ*tal* PKS (VS1024), C) Δ*taL* PKS (VS1025), and D) Δ*talL* double PKS mutant (VS1029). The high detection ability of the LC/MS analysis revealed miniscule levels of **1** in Δ*tal* and Δ*taL* mutants (see Experimental Section). Nevertheless, deletion of both PKS-encoding genes in Δ*talL* mutants led to complete abolishment of myxovirescin production. E) MS-MS fragmentation pattern of **1**.

achieve antibiotic resistance,[39] or to tolerate their own phytotoxins.[40] The GNAT domain of the myxovirescin gene cluster shows close similarity to such domains found in the onnamide, pederin, and curacin A biosynthetic systems.[9,41,42] However, the function of GNAT domains in these systems remains obscure. Although the GNAT domain in myxovirescin biosynthesis could catalyze the transfer of the starter moiety to the nitrogen atom of glycine, a more likely candidate for this reaction is the C domain of the NRPS module of Ta-1 (see below).

Starter biosynthesis could be initiated by loading of CoA-activated acetate and malonate onto the two ACPs of TaI by the TaV trans-ATs, each of which might be responsible for transferring one substrate. Next, the TaI KS might catalyze their decarboxylative condensation to form an acetoacetyl–ACP (Scheme 2).

The other PKS, TaL, consists of KS–KR–ACP–KS–ACP domains. The first KS domain of TaL (TaL-KS1) contains a His to Gln substitution in the conserved box 2 (Figure 3 A), which most likely renders it inactive as a condensing enzyme.[29] This mutant KS, referred to in the text as $KS^{H/Q}$, should be distinguished from $KS^{Q}$ synthase mutants which have characteristic active-site Cys to Gln substitutions.[43,44] The $KS^{H/Q}$ mutation, also observed in KS1 of MmpA of the mupirocin biosynthetic gene cluster, was shown to be indispensable for mupirocin production, both by deletion of the whole KS domain and by point mutation of the active-site Cys to Ala. El-Sayed et al. proposed that $KS^{H/Q}$ might act as a pseudo-loading module that either enables the transfer of an intermediate from MmpD to MmpA or loads the starter on MmpD.[11] Whereas $KS^{H/Q}$ could help to load the acetyl–CoA onto TaL–ACP1, $KS^{H/Q}$-mediated transfer of intermediates from TaI to TaL is not plausible because it would increase the length of the presumed starter unit from 4 to 6 carbons. Finally, TaL-KS2 might catalyze decarboxylative condensation of acetyl–S–ACP and malonyl–S–ACP to yield acetoacetyl–ACP.

Irrespective of whether TaI or TaL performs the first biosynthetic step of fusing acetyl–S–ACP with malonyl–S–ACP, both PKSs lack adequate biosynthetic domains that are needed for the full reduction of the C2 carbon. This suggests an additional interplay of "trans"-acting reductive domains in starter assembly. SAM-derived methylation at the C1 position might be carried out by TaS (Table 1) early during starter biosynthesis, whereas oxygenation of C3 could be carried out by the TaJ monooxygenase, the gene for which is found to be transcriptionally coupled to *taL* (Scheme 2).

To find out which PKS carries out the first biosynthetic step, we have separately deleted ACP–KS–KR–ACP coding regions of *tal* and ACP–KS–ACP coding regions of *taL* (Table 3), and analyzed production of **1** in the resulting mutants. To our surprise,

  

**Table 4.** NMR data of **3** in $CDCl_3$.

| Carbon | $^{13}C$ | $^{1}H$ *J* (Hz) | *m* | Carbon | $^{13}C$ | $^{1}H$ *J* (Hz) | *m* |
|---|---|---|---|---|---|---|---|
| 1 | 18.1 | 1.36 | m | 18 | 21.8 | 1.69 | m |
| | | | | | | 1.34 | m |
| 2 | 34.2 | 1.82 | m | 19 | 42.9 | 2.40 | m |
| | | | | | | 2.22 | m |
| 3 | 73.2 | 5.24 | m | 20 | 212.5 | – | – |
| 4 | 171.6 | – | – | 21 | 42.4 | 2.39 | m |
| 5 | 44.8 | 3.5 | m | 22 | 23.5 | 1.53 | m |
| 6 | 69.8 | 3.96 | m | 23 | 26.5 | 1.24 | s |
| | | | | | | 1.14 (7) | d |
| 7 | 37.4 | 2.12 | m | 24 | 36.6 | 1.34 | m |
| | | 1.48 | m | | | 1.06 | m |
| 8 | 71.8 | 3.6 | m | 25 | 30.2 | 1.24 | s |
| 9 | 80.0 | 3.3 | m | 26 | 41.2 | 1.63 | m |
| | | | | | | 1.28 | m |
| 10 | 29.4 | 2.09 | m | 27 | 36.8 | 2.60 | m |
| | | 1.37 | m | | | | |
| 11 | 31.9 | 2.5 | m | 28 | 175.8 | – | – |
| | | 2.26 | m | | | | |
| 12 | 146.4 | – | – | 29 | 108.3 | 4.79 | s |
| | | | | | | 4.77 | s |
| 13 | 80.6 | 4.21 (9) | d | 30* | 34.2 | 1.82 | m |
| 14 | 129.2 | 5.50 (15/8) | dd | 31 | 12.0 | 0.84 (7) | t |
| 15 | 139.7 | 5.30 (15/11) | dd | 32 | 13.7 | 0.92 (7) | t |
| 16 | 45.1 | 1.89 | m | 33 | 17.4 | 1.14 (7) | d |
| 17* | 34.11 | 1.41 | m | 34 | 20.0 | 0.85 (7) | d |
| | | 1.09 | m | | | | |

* indicates interchangeable carbons.

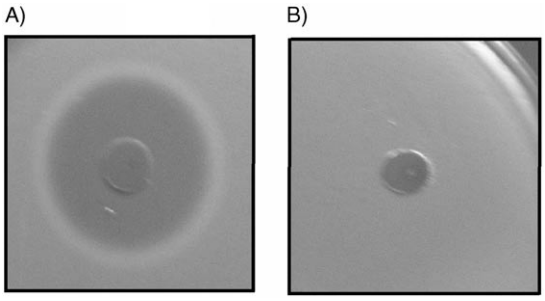


**Figure 5.** A) Antibiotic-activity test performed with myxovirescin A (10 μg) and B) its desmethyl analogue **3**, which were spotted on a filter disc and layered on the lawn of *E. coli* XL-1 blue cells. The lack of inhibition by **3** suggests the indispensability of *O*-specific methylation for the antimicrobial activity of the myxovirescin antibiotic.

quantitative LC-MS analysis of both Δ*tal* and Δ*taL* extracts indicated approximately 100 000-fold reduction in myxovirescin production compared to the wild-type strain. To further clarify whether precursor biosynthesis is dependent on the presence of TaI and TaL PKSs, channeled from the metabolic pool, or simply a product of another PKS encoded in the genome, a double Δ*talL* mutant was created (Table 3). The complete loss of myxovirescin production in Δ*talL* mutants (Figure 4D) rules out the second and third possibility and indicates the direct involvement of TaI and TaL PKSs in starter biosynthesis. Furthermore, basal levels of **1** in Δ*tal* and Δ*taL* and its absence in Δ*talL* mutants argue that either PKS (TaI or TaL) is adequate for starter biosynthesis and myxovirescin production, and eliminates the possibility of transfer of an intermediate from TaI to TaL during biosynthesis. Moreover, involvement of TaI and TaL in later steps of polyketide assembly seems equally unlikely due to the good agreement of the proposed biosynthetic pathway with the enzymatic functions of Ta-1, TaO, and TaP (see below). Finally, the dramatic reductions of myxovirescin production in Δ*tal* and Δ*taL* mutants suggests that both TaI and TaL are required for wild-type levels of antibiotic production—possibly by adding to the structural stability of the myxovirescin megasynthetase.

### Assembly of myxovirescin A combines HMG–CoA synthase and PKS/NRPS enzymology

Following biosynthesis of the putative starter moiety, 2-hydroxyvaleryl–S–ACP, the NRPS module located at the N terminus of Ta-1 extends this molecule with glycine. The adenylylation domain shows a very good agreement with the conserved core region that is specific for activation of glycine (DILQLGMIWK).[45] This confirms the results obtained from isotope-labeling experiments.[27] Consistent with **1**, modules 1 and 2 are expected to follow typical PKS assembly-line logic to yield intermediate **5** (Figure 6).

Module 3 consists of an ACP with the conserved active-site Ser, and a $KS^{H/Q}$ β-ketosynthase, which is thought to be capable of binding the intermediate to the active-site Cys, but which is defective in decarboxylation of the substrate required for elongative condensation (see above). Even though module 3 is not likely to be involved in the extension of **5**, it might be involved in the transfer of the acyl chain to module 4 either through $KS3^{H/Q}$ and ACP3, or directly through ACP3. Mutagenesis studies performed on $KS1^{H/Q}$ of the mupirocin system have shown that its active-site Cys is essential for mupirocin production.[11] In addition, the above hypothesis is also supported by extensive studies of the PikAIV PKS that harbors the last module (module 6) of the pikromycin PKS. This module was thought to be skipped when the shorter, 10-deoxymethynolide hexaketide was produced instead of the heptaketide narbonolide. However, contrary to expectations, active-site mutagenesis (KS, AT, and ACP) of module 6 proved essential, leading to a model that proposed transacylation of the product by KS6 and ACP6 without its subsequent elongation.[46]

If it is not transferred by module 3, **5** might alternatively be moved directly from ACP2 to KS4 and thereby completely by-

  

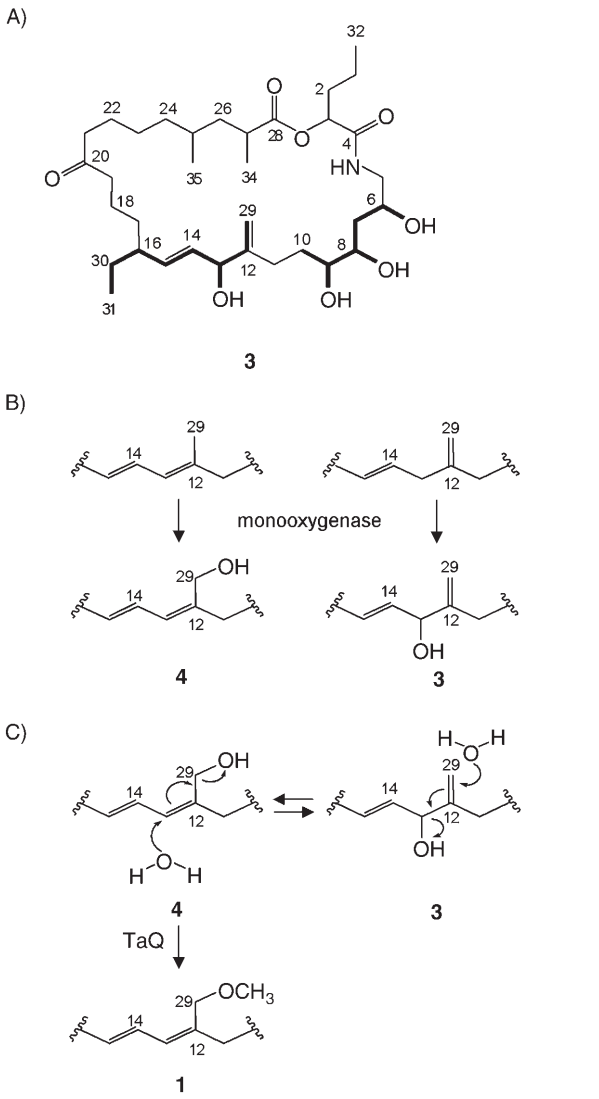


**Scheme 1.** A) Structure of a novel desmethyl analogue of myxovirescin A (**3**) elucidated by NMR spectroscopy. The bonds shown in bold indicate two fragments deduced from $^{1}H,^{1}H$ COSY. B) Hydroxylations of two postulated intermediates that result from PKS/HMG–COA reactions. According to the first possibility, hydroxylation at C29 of the diene-containing myxovirescin precursor produces intermediate **4**, whereas hydroxylation at C13 of the *exo*-methylene-like myxovirescin precursor yields **3**. C) Hypothetical conversion of **3** into **4** and vice versa, which could take place either by enzymatic or nonenzymatic isomerization, might explain the existence of **3** as the main structure revealed by NMR spectroscopy. In wild-type cells, **4** acts as a substrate for TaQ to yield mature myxovirescin A (**1**).

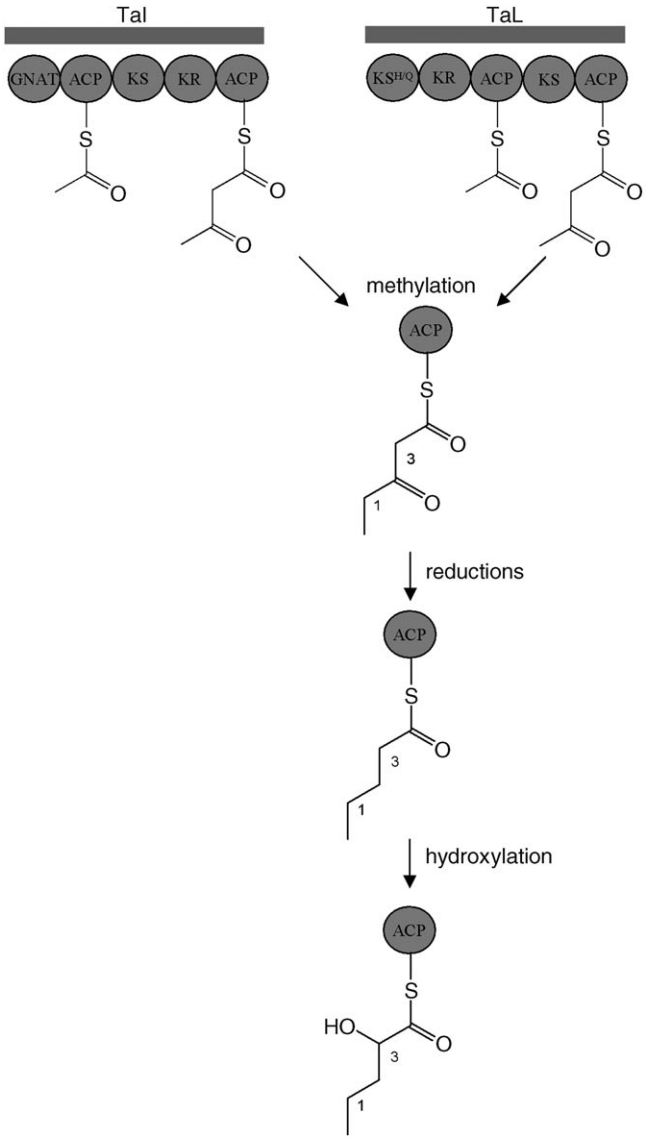


**Scheme 2.** Two possible routes to starter biosynthesis. Both TaI and TaL could catalyze the first biosynthetic reaction of fusing acetyl–S–ACP with malonyl–S–ACP to yield acetoacetyl–ACP. Acetoacetyl–ACP would have to undergo methylation at C1, followed by reductions of C2, and final hydroxylation at C3 to yield the C3-hydroxyvaleryl–ACP starter.

passes module 3. An example for such a mechanism was recently found in the NRPS system that encodes for myxochromide S, in which module 4 was shown to be completely skipped during biosynthesis.[47]

Following transfer of **5** to KS4, module 4 is proposed to contribute with another extension unit while performing β-ketoreduction and dehydration on C10, whereas minimal module 5, which consists of only KS and ACP domains, leads to the formation of intermediate **6**. The isotope labeling scheme, which indicates the addition of a C2 atom of acetate at carbon C12 (Figure 2 A), and structural analogy of intermediate **6** with ace-

**Figure 6.** The proposed biosynthesis pathway of myxovirescin A switches two times from PKS to HMG–CoA synthase biochemistry. The enzymatic domains are: KS: β-ketosynthase, KS$^{H/Q}$: nonfunctional KS, AT: acyltransferase, KR: ketoreductase, DH: dehydratase, ER: enoylreductase, MT: methyltransferase, ACP: acyl-carrier protein, TE: thioesterase, C: condensation domain, A: adenylylation domain, PCP: peptidyl-carrier protein, HMG: 3-hydroxy-3-methylglutaryl synthase, ECH: enoyl–CoA hydratase, KS$^{S}$: decarboxylase. Intermediate **6** attached to ACP5 is shown in abbreviated form to accentuate its resemblance to acetoacetyl–CoA. During the first round of "HMG-box" reactions, TaC is predicted to add acetate onto the β-keto position of **6**, while the KS$^{S}$, TaK, performs sequential decarboxylation and dehydration. The modified product undergoes final isomerization by the TaX enoyl–CoA hydratase to yield intermediate **7**. Intermediate **7** is then subjected to two more rounds of PKS extensions directed by modules 6 and 7 to form intermediate **8**. In the second round of HMG-box reactions, TaF adds propionyl–CoA onto the β-keto position of **8**, TaK KS$^{S}$ carries out the second round of decarboxylation and dehydration reactions, while the second enoyl–CoA hydratase/isomerase, TaY, performs the final isomerization to yield intermediate **9**.

  

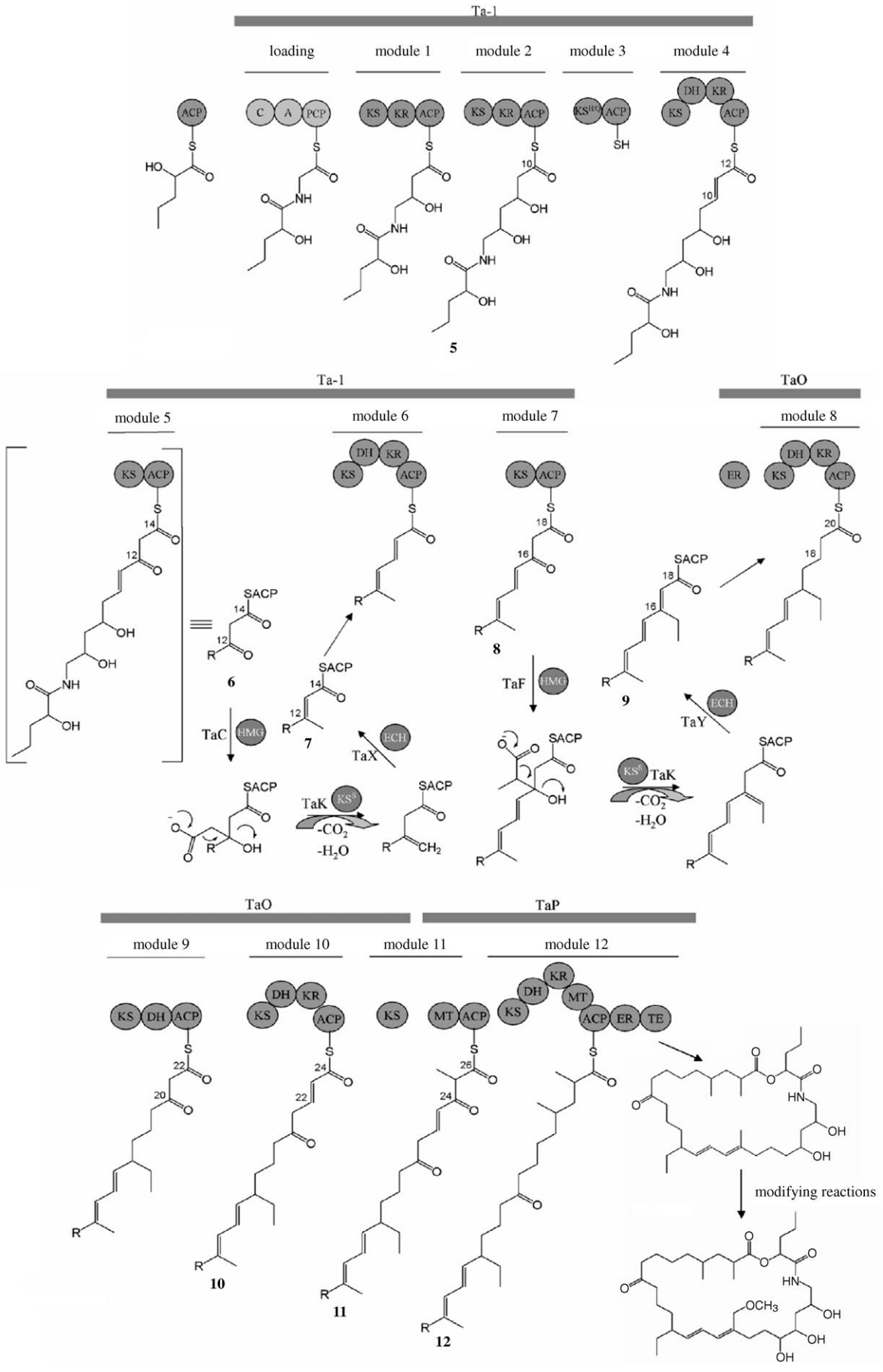


  

toacetyl–CoA (Figure 6), suggest that intermediate **6** might be the substrate of a HMG–CoA synthase-like enzyme.

HMG–CoA synthases perform Claisen condensation by mediating the attack of acetyl–CoA on the β-keto group of acetoacetyl–CoA.[36] Following addition of acetate at the C12 keto carbon of **6**, sequential decarboxylation, water elimination (possibly involving activation of the hydroxyl group), and isomerization reactions would be required to obtain intermediate **7**. In our model, TaC HMG–CoA synthase is depicted to add acetate, TaK β-keto synthase with the Cys to Ser active-site substitution ($KS^S$) would carry out the decarboxylation, and the enoyl–CoA hydratase (ECH), TaX, would perform the isomerization reactions (Figure 6). The assignment of TaK as decarboxylase was based on biochemical studies of Cys to Ser KS point mutants in *E. coli*. For instance, a Cys to Ser mutant of KSI was shown to bind and decarboxylate myristic acid. However, the enzyme's ability to perform elongation condensation was severely compromised.[48] In addition, a Cys to Ser mutant of *E. coli* KSIII exhibited a 425% higher decarboxylation activity than the wild type.[49] Decarboxylation enzymes such as $KS^S$ might be needed to compensate for the presence of a poor leaving group, such as hydroxyl, which is found in the proposed intermediate (Figure 6). In the mevalonate pathway this situation is circumvented by activation of the hydroxyl by phosphorylation.[50] However, no gene encoding for a hypothetical kinase could be found in the myxovirescin gene cluster.

Modules 6 and 7, which encode the same repertoire of catalytic domains as modules 4 and 5, are expected to yield compound **8**. This intermediate, which is attached to the ACP located at the C terminus of the Ta-1 megasynthetase, is presumed to act as a nucleophile in the second reaction catalyzed by a HMG–CoA synthase; the latter now uses propionyl–CoA instead of acetyl–CoA as substrate (see below). Addition of propionyl–CoA onto C16 by HMG–CoA synthase (TaF) followed by sequential decarboxylation (TaK), water elimination, and isomerization (TaY) are hypothesized to give rise to intermediate **9**.

Conclusive data confirming the incorporation of propionate rather than acetate at carbon C16 came from the analysis of $^{13}C$ NMR spectra obtained from myxovirescin-producing *M. virescens* strain Mx v48 that were fed with [2,3-$^{13}C_2$]-succinate. This experiment indicated incorporation of an intact [2,3-$C_2$]-succinate-derived unit into **1**, which was likely achieved by conversion of succinyl–CoA into propionyl–CoA.[16]

$KS^S$ and ECH homologues have been found in all natural product biosynthetic gene clusters that harbor HMG–CoA synthases,[11,12,28,42,51] and HMG–CoA synthase-based mechanisms for the incorporation of methyl groups have been proposed for mupirocin and pederin biosynthesis.[11,10] However, myxovirescin is the first system where a HMG–CoA synthase (TaF) is postulated to act upon a substrate other than acetyl–CoA, and to contain two HMG–CoA synthases (TaC and TaF) and two enoyl–CoA hydratases (TaX and TaY). Nevertheless, only one decarboxylative enzyme $KS^S$ (TaK) is present in the cluster and is depicted to act after both HMG–CoA synthases. Similar to models published recently by Gerwick's group for curacin and jamaicamide biosynthesis,[12,42] the two isomerization reactions are thought to be carried out by TaX and TaY enoyl–CoA hydratases/isomerases.

After the second round of HMG–CoA-like modifications, biosynthesis switches back to PKS biochemistry. Intermediate **8**, which is attached to ACP7 of Ta-1, is further reduced by the ER domain of TaO and transferred to module 8 where another extension with malonyl–S–ACP, keto reduction, and dehydration is performed. The ER domain encoded prior to module 8 is expected to complete this set of reductive reactions. Module 9 (KS–DH–ACP) is predicted to extend the polyketide with one more malonyl–S–ACP unit. Although DH9 contains the conserved active site, it is unlikely to act without a KR domain. This observation is consistent with the intact keto functionality at C20 of myxovirescin A. Further, module 10 (KS–DH–KR–ACP) introduces the next malonyl–S–ACP unit followed by β-keto-reduction at C22.

Module 11 is physically split between TaO and TaP PKSs (Figure 6) and the KS domain of TaP is most likely complemented with MT and ACP domains of TaO to create a functional module 11. To eliminate the possibility of a frame shift due to errors in sequencing, a 0.84 kb region covering the end of *taO* and beginning of *taP* was cloned and resequenced (Experimental Section). The results confirmed the validity of the sequence. Furthermore, this module lacks reductive domains that are expected to saturate C24.

Finally, module 12 has the full reductive capacity to saturate the C26 keto group, while the MT domain is most likely responsible for methylation of C27. In the last step, the linear product attached to ACP12 undergoes cyclization by nucleophilic attack of the C3 hydroxy oxygen onto the C28 carbonyl to generate the basic myxovirescin lactone fold.

### Reductive reactions

Three out of nine ketoreductase domains contain alterations in the Rosmann fold (GxGxxG). KR1 and KR4 contain a conserved Gly to Ala substitution (GxGxxA), which is also present in KR1 and KR2 of avermectin.[52] KR2 has a nonconserved Gly to Arg substitution, which judging from several KRs with the identical substitution, is also most likely to be active.[53,54]

The myxovirescin gene cluster harbors only two out of the five expected ER domains, and three double bonds, C10=C11, C16=C17, and C22=C23, as well as the C24 keto group, require reduction (Figure 6). It is interesting to notice that the two ERs take unusual positions within PKS modules; one ER, for example, precedes KS8. Taking into account that, typically, the start of a module is defined with a KS and its end with an ACP or TE domain, this ER cannot be functionally assigned to either module 7 (KS–ACP) or module 8 (KS–DH–KR–ACP), to which it translationally belongs. However, our hypothetical scheme suggests a need for enoylreductase within both modules 7 and 8. Accordingly, the first enoyl reduction would saturate the C16=C17 double bond of intermediate **9**, while the second reduction would occur after extension of **9** by module 8 and aid KR8 and DH8 in the full reduction of the C18 ketone. Therefore, the ambiguous positioning of the ER domain at the interface of

  

modules 7 and 8, along with our proposed assembly scheme, raises the possibility that this ER is actively shared by two modules that are encoded on two proteins.

Further, analysis of modules 10 and 11 suggests that module 10 "lacks" an ER domain that is needed for saturating the C22=C23 double bond. Furthermore, the "split" module 11, in TaO and TaP PKSs, "lacks" a complete reductive loop that is expected to saturate the C24 ketone. However, the last module (module 12) contains all three reductive domains, with the ER unusually positioned between the ACP and TE domains. We postulate that all the above-mentioned reductive reactions take place on intermediate **12** within module 12. This model would explain the physical separation of the ER from the KR and DH domains within this module, and would allow the domain to act iteratively and independently of the other two reductive domains. Alternatively, intermediates **10** and **11** would have to skip from their respective modules to module 12 and back, in order to achieve the expected reductions before the intermediates are passed to module 12 for the final cycle of extension and modification.

#### Split modules and shared domains

Besides the presence of HMG–CoA synthases, $KS^S$ and ECH (HMG–CoA box), and irregularly distributed reductive domains, the complexity of myxovirescin programming is also evident in the occurrence of modules that appear on two proteins and, therefore, can be classified as "split". This situation is encountered in module 11 where the KS domain encoded at the C terminus of TaO is likely complemented with MT and ACP domains of TaP. Split modules are encountered rather frequently in myxobacterial natural product clusters.[33,34,55]

Module 7 can also be considered as split as it consists of KS and ACP domains, which are presumably complemented by the HMG box, and finally reduced by the ER domain of TaO. In this particular case, the need for a split module is well rationalized with the proposed reaction mechanism, which suggests the interference of the HMG–CoA box in product assembly, and therefore requires an intact acetoacetyl–S–ACP-like intermediate. However, the "irregular" positioning of the ER domain at the interface of modules 7 and 8 can also be regarded as a "shared domain".

#### Auxiliary modifications

In addition to the required oxygenation at the C3 position—most likely carried out by the TaJ monooxygenase—two more oxidative enzymes, TaH cytochrome P450-dependent oxygenase and TaN dioxygenase (Table 1), are expected to perform hydroxylations at C9 and C29. MT11 and MT12, encoded within the TaP PKS, are expected to methylate carbons C25 and C27.

By inactivating *taQ* in *M. xanthus* DK1622, we were able to demonstrate a shift in the production of **1** and **2** toward two novel metabolites (Figure 1C). Furthermore, NMR analysis of the novel compound with *m/z* 610 $[M+H]^+$ has revealed the loss of the methoxy group specific to C29. Therefore, this provides clear evidence that TaQ functions as the *O*-methyltransferase (Scheme 1A). However, contrary to the predicted hydroxyl functionality connected to C29, NMR analysis of **3** revealed an *exo*-methylene specific to this position, whereas the hydroxyl group was found to be attached to carbon C13 (Scheme 1A).

Since either an *exo*-methylene or a diene intermediate might be produced by the HMG–CoA-dependent addition of the methyl group (Figure 6), two options that lead to myxovirescin A biosynthesis can be envisioned (Scheme 1B). The first possibility is that hydroxylation of the diene-containing intermediate at C29 yields **4**, which serves as a substrate for TaQ to yield myxovirescin A. The second scenario postulates hydroxylation of the *exo*-methylene intermediate at C13 to yield structure **3**, which was defined by NMR spectroscopy. Intermediate **3** could be isomerized to **4** and methylated by TaQ (Scheme 1C). The second pathway suggests a dual role for TaQ as both isomerase and methyltransferase. Therefore, **3** might be a natural precursor of myxovirescin A. Alternatively, **3** can be formed by enzymatic or nonenzymatic transformation of **4** in the absence of TaQ methyltransferase.

Finally, the methylation at C1 could be attributed to TaS—the enzyme that shows homology with members of the radical SAM-protein superfamily. This superfamily encompasses a wide range of enzymes, some of which function as methyltransferases.[56] The involvement of *taS* in myxovirescin production remains to be proven in further experiments.

## Conclusion

Myxovirescin megasynthetase shows a number of unusual features such as a dual pathway dedicated to starter biosynthesis, multimodular AT-less megasynthetases with trans-acting acyltransferases, lack of reductive domains, "split" modules, and a thioesterase that is not directly preceded by an ACP. In addition, the gene cluster is comprised of a number of noncanonical PKS enzymes and domains (GNAT, HMG–CoA synthases, and enoyl–CoA hydratases) and a β-ketosynthase that has a Cys to Ser point mutation. All these features challenge our previous knowledge pertaining to the organization of PKSs, their colinearity, and classification.

The myxovirescin biosynthetic gene cluster belongs to the novel family of natural-product gene clusters that is comprised of pederin, mupirocin, onnamide, curacin A, and jamaicamide. All clusters within this family appear to have acquired a novel variation in natural-product assembly by combining PKS/NRPS assembly lines with HMG–CoA synthase-type biochemistry. Elucidation of the biosynthetic logic that governs PKS/NRPS/HMG–CoA-orchestrated assembly of natural products will not only enrich the lexicon of natural-product biochemistry with another chapter, but more importantly, pave the way to designing novel antitumor and antibiotic analogues by using the HMG–CoA toolbox. The myxovirescin system of *M. xanthus* provides an excellent molecular-genetic platform for such studies.

  

## Experimental Section

**Growth media**: *M. xanthus* strain DK1622 was grown in casitone yeast extract (CYE) medium that consisted of casitone (10%; Difco), yeast extract (5%; Difco), $MgSO_4 \cdot 7H_2O$ (0.1%), and 3-morpholinopropanesulfonic acid buffer (MOPS; 10 mM) at pH 7.6. Myxovirescin production was assayed in MD-1 medium that consisted of casitone (0.3%), $CaCl_2 \cdot 2H_2O$ (80.07%), and $MgSO_4 \cdot 7H_2O$ (0.2%); vitamin B12 ($5 \times 10^{-4}$ μg $L^{-1}$) was added after cooling. For cloning purposes *E. coli* strain DH5λ was grown in Luria–Bertani (LB) medium[57] and supplemented with standard amounts of antibiotic as required.

**Annotation of the myxovirescin biosynthetic gene cluster**: The complete sequence of the myxovirescin gene cluster was obtained from TIGR (http://www.tigr.org/tdb). Further annotation of the catalytic domains was performed by using the PKS-NRPS program kindly provided by Jacques Ravel (http://jhunix.hcf.jhu.edu/~ravel/nrps//index2.html). Annotation of the nitrogen-specific acetyltransferase (GNAT) and ACP domains of TaI, KR, and TaL were carried out by using the Pfam search engine (http://pfam.wustl.edu). MT domains were defined by using the natural-product biosynthetic gene database (www.npbiogene.com).

**Construction of in-frame deletion mutants of *taV*, *taI*, *taL*, and *talL***: Construction of in-frame deletion mutants was carried out by amplifying approximately 600 bp regions on each side of the desired deletion area with Taq polymerase. Each fragment was subcloned into the pCR2.1®-TOPO vector (Invitrogen; see Supporting Information for the list of primers used). Following sequencing of the cloned regions, the corresponding amplification products were cut out of the pCR2.1-TOPO vector by using the restriction sites indicated (Table 3). The fragments were then gel purified and cloned into the pSWU41 vector, which carries a neomycin phosphotransferase (*nptII*) and levansucrase (*sacB*) gene cassette. The final constructs were electroporated into *M. xanthus*,[58] and kanamycin-resistant, sucrose-sensitive clones were checked for proper integration of the plasmid by PCR amplification. One transformant which showed the correct genotype was grown in CYE medium for three days with daily dilutions. On the third day, $0.2–2.0 \times 10^8$ cells were mixed with CYE–soft agar (0.75%; 3 mL) and poured onto CYE–agar plates that contained sucrose (5%), and incubated at 30 °C for four days. Well-isolated colonies were picked and transferred onto CYE–agar containing sucrose (5%), and grown at 30 °C for two days before being transferred onto CYE–agar containing kanamycin (40 μg $mL^{-1}$). After two days of growth at 30 °C, colonies that were kanamycin sensitive and sucrose resistant were subjected to chromosomal-DNA extraction and their genotypes were confirmed by PCR amplification. In one PCR reaction a primer pair was used that recognized sequences outside of the region that was initially amplified. This yielded a product that was shorter than the desired deletion. As a negative control, the second PCR reaction was performed with a primer that bound outside of the amplified region in combination with a primer specific for the deletion area. To create a double Δ*talL* mutant, plasmid pVS61 was electroporated into *M. xanthus* VS1024 (Δ*taI*). The excision of the plasmid resulted in *M. xanthus* VS1029.

**Construction of the *taQ* mutant**: To construct a *taQ* knockout, an internal 450 bp of *taQ* was amplified by using Taq polymerase and the primer pair taQ_knock_for and taQ_knock_rev. The former primer contained a base-pair insertion (Supporting Information) that created a stop codon. The PCR product was cloned into pCR2.1-TOPO and sequenced. The resulting plasmid, pVS16, was then electroporated into *M. xanthus* DK1622.[58] Transformants were grown in CYE medium supplemented with kanamycin, and their genomic DNA was analyzed for integration of the plasmid in *taQ* by using PCR amplification. The primers used were taQ_knock_for (specific for *taQ*) and 21down (specific for pCR2.1-TOPO). The *taQ* knockout mutant was named VS1016.

**Analysis of the *taO–taP* intergenic region**: To eliminate the possibility of frame-shift error(s), 0.824 kb that covered the region near the 3′ end of *taO* and the 5′ region of *taP*, was PCR amplified by using Pfu Turbo polymerase (Strategene) and primers taOseq_up and taOseq_down (Supporting Information). Following gel purification of the blunt-ended PCR product, A overhangs were added to it by using Taq polymerase, and the modified PCR product was cloned into pCR2.1-TOPO to create plasmid pVS75. The sequenced region was analyzed for ORFs by using FramePlot 3.0beta software (http://watson.nih.go.jp/~jun/cgi-bin/frameplot-3.0b.pl).

**Fermentation and extraction conditions**: Typically, MD-1 medium (100 mL) that contained amberlite XAD-16 (1%; Rohm & Haas, Frankfurt/Main, Germany) was inoculated with *M. xanthus* ($1.5 \times 10^8$ cells $mL^{-1}$). After 3 days at 30 °C, the cells and XAD beads were centrifuged for 15 min at 10000 *g*. The combined pellet of cells and XAD beads was extracted with methanol (3×50 mL). The total extract was resuspended in methanol (2 mL) and concentrated into 200 μL.

**Antibiotic assay**: In order to test inhibitory activity, *E. coli* XL-1 blue (0.1 mL) at 0.1 $OD_{600}$ were mixed with LB–soft agar (3 mL) and plated on a LB–agar plate. Purified antibiotics (10 μg and 50 μg) were spotted on the filter disk, dried, and placed on the soft agar. The plate was incubated at 30 °C for 24 h.

**Purification of myxovirescins from *M. xanthus* DK1622**: To purify myxovirescins from wild-type *M. xanthus* DK1622, cells (8 L) were grown in a fermentor (Biostat V, Braun) under the conditions described above. At the end of the fermentation, XAD-adsorbent resin was removed by filtration through a 0.2 mm sieve (Retsch, Haan, Germany), and antibiotics were extracted from the resin by using methanol (3×400 mL). The total methanol extract was then applied to a Sephadex LH-20 column (100 cm×2.5 cm) and eluted with methanol. Fractions that tested positive for myxovirescins were concentrated, dissolved in dichloromethane:methanol (15:1; 3 mL), applied to a silica-gel column (780×23 mm), and eluted by using the same solvent system. Fractions that contained myxovirescins were further concentrated, dissolved in methanol, and purified by preparative HPLC by using a Nucleosil 100–7 C-18 column (250×21 mm; Macherey & Nagel, Düren, Germany). Myxovirescins A and C were purified by sequential preparative HPLC (see above) by using different MeOH/$H_2O$ mixtures.

The final yields of myxovirescins A and C were 3 and 5 mg, respectively.

**Purification of myxovirescin Qa from the *taQ* mutant, VS1016**: In order to isolate myxovirescin $Q_a$, *taQ* mutant cells (9 L) were grown in MD-1 medium until the late stationary phase was reached. After centrifugation, cells and XAD were extracted with methanol (3× 400 mL). The total extract was concentrated and separated on a Sephadex LH-20 column. Fractions that tested positive for myxovirescin $Q_a$ ($R_f = 0.375$) were collected, concentrated, and applied to preparative HPLC as described for the purification of myxovirescins A and C, and yielded a total of 2 mg of pure compound.

**Myxovirescin A detection and quantification**: Detection of myxovirescins by TLC was carried out by using a dichloromethane/methanol (15:1) solvent system. Myxovirescins were detected as a dark spot under 254 nm ultraviolet light ($R_f = 0.26$).

  

Additional detection by analytical reversed-phase HPLC was carried out by using the Dionex P680 pump unit coupled to PDA-100 DAD on a RP 125×2 mm/3 μm Nucleodur C-18 column (Macherey & Nagel). Solvent A: $H_2O$ with formic acid (0.1%); solvent B: acetonitrile with formic acid (0.1%); flow rate 0.4 mL min$^{-1}$, and the following program: 0–2 min, 5% B; 2–17 min to 95% B; 17–20 min, 95% B; 20–23 min, 5% B. Under these conditions, myxovirescin A showed a retention time of 15.0 min and a characteristic $UV_{max}$ absorption at 239 nm.

**Liquid chromatography/mass spectrometry (LC/MS) and quantification of myxovirescin A by ion-trap MS**: LC/MS measurements were performed on an Agilent 1100 series system equipped with a photodiode-array detector, and coupled to a Bruker HCT plus mass spectrometer operated in positive-ionization mode at a scan range from *m/z* 100 to 1100. Myxovirescin A showed a characteristic *m/z* 624.3 $[M+H]^+$.

In order to quantify myxovirescin A, combined cell and XAD extracts were separated by RP-HPLC on a 125×2 mm/3 μm Nucleodur C-18 column by using an Agilent 1100 series solvent-delivery system and a flow rate of 0.4 mL min$^{-1}$. The gradient employed the same solvents as used for LC-MS and consisted of 0–1 min 70% B, 1–6 min to 95% B. Under these conditions myxovirescin A displayed a retention time of 3 min. Quantitative analysis was done on a coupled ESI ion-trap MS machine (Bruker HCTplus) operated in the manual MS(n) mode. Ions of *m/z* 624 $[M+H]^+$ were collected and subjected to fragmentation. The intensities of the three fragment ions (592, 574, and 556 $[M+H]^+$) were summed up and peak integration was carried out by utilizing the Bruker QuantAnalysis v1.5 software package. The calibration curve consisted of a series of dilutions of the purified myxovirescin A. Samples under investigation were diluted as required to fit the dynamic range of the method utilized.

**NMR analysis**: NMR analysis was performed in $CD_3OD$ or $CDCl_3$ by using a Bruker Advance 500 instrument. $^1H$ NMR spectra were measured at 500 MHz. $^{13}C$ spectra, $^1H,^1H$ COSY, gradient spectroscopy HSQC, and HMBC data were obtained at 125 MHz. Distortionless enhancement by polarization transfer (DEPT) spectrum was measured at 135°.

## Acknowledgements

*We would like to thank Jacques Ravel for supplying us with the PKS-NRPS software for the analysis of catalytic domains, and Helge B. Bode for helpful comments and critical reading of the manuscript. This work was supported by BMB+F and DFG research grants to R.M.*

**Keywords:** biosynthesis · hybrid polyketide/nonribosomal peptide · natural products · polyketides · trans-acyltransferases

[1] J. Staunton, K. J. Weissman, *Nat. Prod. Rep.* **2001**, *18*, 380–416.
[2] C. T. Walsh, *Science* **2004**, *303*, 1805–1810.
[3] S. A. Sieber, M. A. Marahiel, *Chem. Rev.* **2005**, *105*, 715–738.
[4] B. Silakowski, H. U. Schairer, H. Ehret, B. Kunze, S. Weinig, G. Nordsiek, P. Brandt, H. Blöcker, G. Höfle, S. Beyer, R. Müller, *J. Biol. Chem.* **1999**, *274*, 37391–37399.
[5] S. Smith, A. Witkowski, A. K. Joshi, *Prog. Lipid Res.* **2003**, *42*, 289–317.
[6] J. L. Garwin, A. L. Klages, J. E. Cronan, Jr., *J. Biol. Chem.* **1980**, *255*, 11949–11956.
[7] Y. Ohashi, H. Okuyama, *Biochim. Biophys. Acta* **1986**, *876*, 146–153.
[8] K. Magnuson, S. Jackowski, C. O. Rock, J. E. Cronan, Jr., *Microbiol. Rev.* **1993**, *57*, 522–542.
[9] J. Piel, D. Hui, G. Wen, D. Butzke, M. Platzer, N. Fusetani, S. Matsunaga, *Proc. Natl. Acad. Sci. USA* **2004**, *101*, 16222–16227.
[10] J. Piel, *Proc. Natl. Acad. Sci. USA* **2002**, *99*, 14002–14007.
[11] A. K. El-Sayed, J. Hothersall, S. M. Cooper, E. Stephens, T. J. Simpson, C. M. Thomas, *Chem. Biol.* **2003**, *10*, 419–430.
[12] D. J. Edwards, B. L. Marquez, L. M. Nogle, K. McPhail, D. E. Goeger, M. A. Roberts, W. H. Gerwick, *Chem. Biol.* **2004**, *11*, 817–833.
[13] E. Rosenberg, S. Fytlovitch, S. Carmeli, Y. Kashman, *J. Antibiot.* **1982**, *35*, 788–793.
[14] K. Gerth, H. Irschik, H. Reichenbach, G. Höfle, *J. Antibiot.* **1982**, *35*, 1454–1459.
[15] W. Trowitzsch, K. Gerth, V. Wray, G. Höfle, *J. Chem. Soc. Chem. Commun.* **1983**, 1174–1175.
[16] W. Trowitzsch-Kienast, K. Schober, V. Wray, K. Gerth, H. Reichenbach, G. Höfle, *Liebigs Ann. Chem.* **1989**, 345–355.
[17] A. Manor, I. Eli, M. Varon, H. Judes, E. Rosenberg, *J. Clin. Periodontol.* **1989**, *16*, 621–624.
[18] I. Eli, H. Judes, M. Varon, A. Manor, E. Rosenberg, *Refuat Hashinayim* **1988**, *6*, 14–15.
[19] A. Manor, M. Varon, E. Rosenberg, *J. Dent. Res.* **1985**, *64*, 1371–1373.
[20] Y. Paitan, E. Orr, E. Z. Ron, E. Rosenberg, *FEMS Microbiol. Lett.* **2001**, *203*, 191–197.
[21] Y. Paitan, E. Orr, E. Z. Ron, E. Rosenberg, *Gene* **1999**, *228*, 147–153.
[22] Y. Paitan, G. Alon, E. Orr, E. Z. Ron, E. Rosenberg, *J. Mol. Biol.* **1999**, *286*, 465–474.
[23] Y. Paitan, E. Orr, E. Z. Ron, E. Rosenberg, *J. Bacteriol.* **1999**, *181*, 5644–5651.
[24] Y. Paitan, E. Orr, E. Z. Ron, E. Rosenberg, *FEMS Microbiol. Lett.* **1999**, *170*, 221–227.
[25] H. B. Bode, R. Müller, *Angew. Chem.* **2005**, *117*, 6988–7007; *Angew. Chem. Int. Ed.* **2005**, 44, 6828–6846?.
[26] V. Simunovic, F. C. Gherardini, L. J. Shimkets, *J. Bacteriol.* **2003**, *185*, 5066–5075.
[27] W. Trowitzsch-Kienast, K. Schober, V. Wray, K. Gerth, H. Reichenbach, G. Höfle, *Liebigs Ann. Chem.* **1989**, 345–355.
[28] G. L. Tang, Y. Q. Cheng, B. Shen, *Chem. Biol.* **2004**, *11*, 33–45.
[29] S. W. White, J. Zheng, Y. M. Zhang, C. O. Rock, *Annu. Rev. Biochem.* **2005**, *74*, 791–831.
[30] R. Reid, M. Piagentini, E. Rodriguez, G. Ashley, N. Viswanathan, J. Carney, D. V. Santi, C. R. Hutchinson, R. McDaniel, *Biochemistry* **2003**, *42*, 72–79.
[31] C. D. Reeves, S. Murli, G. W. Ashley, M. Piagentini, C. R. Hutchinson, R. McDaniel, *Biochemistry* **2001**, *40*, 15464–15470.
[32] S. J. Moss, C. J. Martin, B. Wilkinson, *Nat. Prod. Rep.* **2004**, *21*, 575–593.
[33] M. Kopp, H. Irschik, S. Pradella, R. Müller, *ChemBioChem* **2005**, *6*, 1277–1286.
[34] O. Perlova, K. Gerth, A. Hans, O. Kaiser, R. Müller, *J. Biotechnol.* **2005**, *121*, 174–191.
[35] R. M. Kagan, S. Clarke, *Arch. Biochem. Biophys.* **1994**, *310*, 417–427.
[36] N. Campobasso, M. Patel, I. E. Wilding, H. Kallender, M. Rosenberg, M. N. Gwynn, *J. Biol. Chem.* **2004**, *279*, 44883–44888.
[37] W. Trowitzsch, V. Wray, K. Gerth, G. Höfle, *J. Chem. Soc. Chem. Commun.* **1982**, 1340–1341.
[38] Y.-Q. Cheng, G.-L. Tang, B. Shen, *Proc. Natl. Acad. Sci. USA* **2003**, *100*, 3149–3154.
[39] J. Davies, G. D. Wright, *Trends Microbiol.* **1997**, *5*, 234–240.
[40] H. He, Y. Ding, M. Bartlam, F. Sun, Y. Le, X. Qin, H. Tang, R. Zhang, A. Joachimiak, J. Liu, N. Zhao, Z. Rao, *J. Mol. Biol.* **2003**, *325*, 1019–1030.
[41] J. Piel, G. P. Wen, M. Platzer, D. Q. Hui, *ChemBioChem* **2004**, *5*, 93–98.
[42] Z. Chang, N. Sitachitta, J. V. Rossi, M. A. Roberts, P. Flatt, J. Jia, D. H. Sherman, W. H. Gerwick, *J. Nat. Prod.* **2004**, *67*, 1356–1367.
[43] A. Witkowski, A. K. Joshi, Y. Lindqvist, S. Smith, *Biochemistry* **1999**, *38*, 11643–11650.
[44] C. Bisang, P. Long, J. Cortes, J. Westcott, J. Crosby, A.-L. Matharu, R. Cox, T. Simpson, J. Staunton, P. Leadlay, *Nature* **1999**, *401*, 502–505.
[45] T. Stachelhaus, H. D. Mootz, M. A. Marahiel, *Chem. Biol.* **1999**, *6*, 493–505.
[46] B. Beck, Y. Yoon, K. Reynolds, D. Sherman, *Chem. Biol.* **2002**, *9*, 575–583.
[47] S. Wenzel, P. Meiser, T. Binz, T. Mahmud, R. Müller, *Angew. Chem.* **2006**, *118*, 2354–2360; Angew. Chem. Int. Ed. **2006**, 45, 2296–2301.

  

[48] K. A. McGuire, M. Siggaard-Andersen, M. G. Bangera, J. G. Olsen, P. von Wettstein-Knowles, *Biochemistry* **2001**, *40*, 9836 – 9845.
[49] C. Davies, R. J. Heath, S. W. White, C. O. Rock, *Structure* **2000**, *8*, 185 – 195.
[50] G. Michal, *Biochemical Pathways, Vol. 1*, Spektrum, Heidelberg, **1999**.
[51] F. Kunst, N. Ogasawara, I. Moszer, et al., *Nature* **1997**, *390*, 249 – 256.
[52] H. Ikeda, T. Nonomiya, S. Omura, *J. Ind. Microbiol. Biotechnol.* **2001**, *27*, 170 – 176.
[53] K. Nakajima, A. Yamashita, H. Akama, T. Nakatsu, H. Kato, T. Hashimoto, J. Oda, Y. Yamada, *Proc. Natl. Acad. Sci. USA* **1998**, *95*, 4876 – 4881.
[54] M. Fisher, S. E. Sedelnikova, W. Martindale, N. C. Thomas, J. W. Simon, A. R. Slabas, J. B. Rafferty, *Acta Crystallogr. Sect. D Biol. Crystallogr.* **2000**, *56*, 86 – 88.
[55] B. Silakowski, G. Nordsiek, B. Kunze, H. Blöcker, R. Müller, *Chem. Biol.* **2001**, *8*, 59 – 69.
[56] H. J. Sofia, G. Chen, B. G. Hetzler, J. F. Reyes-Spindola, N. E. Miller, *Nucleic Acids Res.* **2001**, *29*, 1097 – 1106.
[57] J. Sambrook, E. F. Fritsch, T. Maniatis, *Molecular Cloning: A Laboratory Manual*, 2nd ed., Cold Spring Harbor Laboratory Press, New York, **1989**.
[58] K. Kashefi, P. L. Hartzell, *Mol. Microbiol.* **1995**, *15*, 483 – 494.

Received: February 25, 2006
Published online on July 11, 2006

  